The Journal of Physical Chemistry B

 VOLUME 102, NUMBER 44, OCTOBER 29, 1998

FEATURE ARTICLE

# Simulations of $H_2O$ Solid, Liquid, and Clusters, with an Emphasis on Ferroelectric Ordering Transition in Hexagonal Ice

**V. Buch* and P. Sandler**

*Department of Physical Chemistry and the Fritz Haber Research Center, The Hebrew University, Jerusalem 91904, Israel*

**J. Sadlej**

*Department of Chemistry, University of Warsaw, 02-093 Warsaw, Poland*

*Received: January 23, 1998; In Final Form: July 8, 1998*

Simulations are presented of $H_2O$ ice, liquid, and clusters $(H_2O)_n$ $n \leq 7$. The first part is devoted to orientational energetics of ice. Ordinary hexagonal ice is orientationally disordered; a transition to an ordered form (ice XI) can be induced at 72 K. The recently demonstrated ferroelectric structure of ice XI (Jackson, S. M.; Wield, V. M.; Whitworth, R. W.; Oguro, M.; Wilson, C. *J. Phys. Chem. B* 1997, *101*, 6142) seems to contradict our understanding of $H_2O\cdots H_2O$ interactions. A polarizable water potential is proposed that accounts qualitatively for the existence of ferroelectric ice XI; its crucial ingredient is the location of the polarizability center. This potential is then tested in classical trajectory simulations of water structure, energetics, self-diffusion, and dielectric constant. Cluster energetics and rotational constants are calculated using the rigid body diffusion Monte Carlo technique.

## 1. Introduction

$H_2O$ has been and remains one of the most extensively studied substances. The reason, of course, is its importance in nature: $H_2O$ is a major constituent of living creatures on earth, of the earth itself, of other solar system bodies, and of interstellar space. Moreover, $H_2O$ is an interesting and unusual substance. Its unique properties are due predominantly to the ability of water molecules to form four relatively strong hydrogen bonds to its neighbors in an approximately tetrahedral arrangement. The arrangement is flexible, resulting in a variety of unique and striking condensed phase properties and phenomena. In addition to $H_2O$ liquid (which is also the most important solvent in nature), $H_2O$ exists, or can be prepared, in 11 distinct solid crystalline forms, and in a range of amorphous forms.[1]

It is then not surprising that a very large body of research has been devoted to molecular level understanding of $H_2O$. Still, this fascinating substance is far from being well understood, and continues to puzzle us with striking physical behaviors. Here, several computer simulation techniques are applied to the modeling of $H_2O$ solid, liquid, and clusters. The emphasis is on understanding the energetics of a phase transition from ordinary hexagonal ice to a ferroelectric form of ice, which seems to defy our understanding of intermolecular $H_2O\cdots H_2O$ interactions.[2,3] We construct a "reasonable" water potential that accounts qualitatively for the existence of this form of ice. This potential is then tested against other $H_2O$ properties.

We start with a brief general introduction to modeling of intermolecular interactions in $H_2O$. Molecular level interpretation of experimental data on various forms of $H_2O$ has profited greatly from computer simulations, and therefore much effort was invested over the years in constructing good water potential energy surfaces (PES).[4,5] (We note at this point that the per-

10.1021/jp980866f CCC: $15.00 
Published on Web 10/07/1998

tinent literature on $H_2O$ is very extensive, and would comprise a reference list of unreasonable length; therefore, the reference list includes only a representative set, most directly relevant to the present discussion.) The hydrogen bond in water and other substances is sometimes viewed as some kind of separate "semichemical" entity. However, simulations suggest that the hydrogen bond can be viewed simply as a relatively strong electrostatic interaction between polar molecules. Many interesting results were obtained with the help of pair-additive potentials, whose chief ingredients were coulombic interaction between point charges distributed on the water molecules, plus terms representing the "hard core" and the van der Waals interaction.[4] It was, however, recognized early on that $H_2O$ monomer properties vary in response to local environments; most notably, $H_2O$ molecules become polarized in condensed phases. This problem was addressed using "effective" pair potentials reflecting average condensed phase monomer properties, rather than gaseous monomer properties. Recently, computer technology improved to the point at which routine simulations employing polarizable non-pair-additive potentials became possible,[5] giving hope for a unified description of all water phases: gas, liquid, solid, clusters, and interfaces.

Most of the past effort in parameterizing water potentials has been directed towards reproducing liquid properties, which contain averaged information on the PES in a broad range of hydrogen bonding configurations. Presently, our understanding of water PES is challenged by a new and exciting set of experimental data on size-selected $(H_2O)_n$ clusters up to $n = 10$.[6−10] Clusters probe PES regimes corresponding to distorted H-bonding, in asymmetric molecular environments. Finally, crystalline ice properties constrain the PES in regions of deep potential minima.[4b,5f,5i,11] The different crystal forms probe selectively narrow and well defined ranges of configurations; in particular, the region of nearly perfect tetrahedral coordination is probed by hexagonal and cubic ice.[1]

In the present study we attempt to reproduce a broad range of $H_2O$ ice, liquid, and cluster properties in the framework of a relatively simple polarizable PES. *Much of our effort is, however, devoted to a single $H_2O$ property, which seems particularly hard to reproduce.* This property pertains to a striking new result published recently on the orientational order−disorder transition in hexagonal ice,[3] and will be explained below in some detail.

It should be noted first that the ordinary hexagonal ice (ice Ih) is a *disordered* substance (see Figure 1). While the O-atoms form a periodic pattern, *molecular orientations are quasirandom* within the so-called ice rules (two chemically bonded and two hydrogen bonded H-atoms around each O-atom).[1] Because of the disorder, ice Ih has finite entropy (0.81 cal/(mol K)) at 0 K.[1b] Pauling[12] showed that one can reproduce this entropy value while assuming that all configurations consistent with the ice rules contribute to it equally. One expects, of course, one (or some) of the configurations to be lower in energy than the "typical" disordered ones; however, orientational ordering is inhibited by freezing of orientational mobility above 100 K.[13] Ordering of portions of ice Ih can be induced at 72 K by introduction of KOH impurity to ice;[2] apparently, the ions keep water molecules orientationally mobile down to this phase transition temperature.

The question as to what is the most stable *ordered* form of ice Ih was addressed by a number of theorists. Several studies[14,15] suggested as the most stable a zero-dipole form $Pna2_1$ shown in Figure 2 (top). This suggestion is supported by a simple qualitative argument: In ice, the nearest neighbor (nn) configuration of water molecules can be either cis or trans[16] (see Figure 3). Trans is energetically more favorable than cis because of the reduced repulsion between the nonbonded

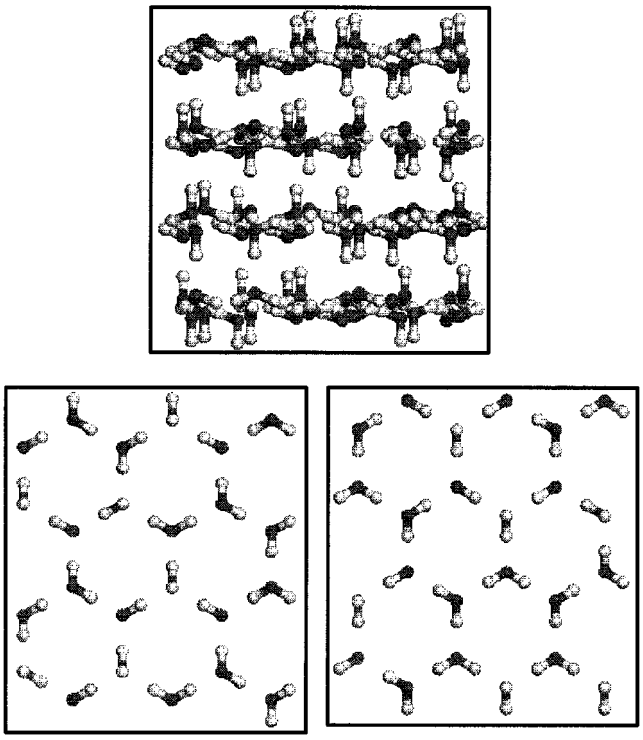

**Figure 1.** A 96-molecule model of "disordered" ice Ih (idealized model, no structural relaxation). Bottom: projections of two of the four hexagonal bilayers on the plane perpendicular to the *c*-axis. Top: "side view" of the the four hexagonal layers; *c*-axis is vertical.

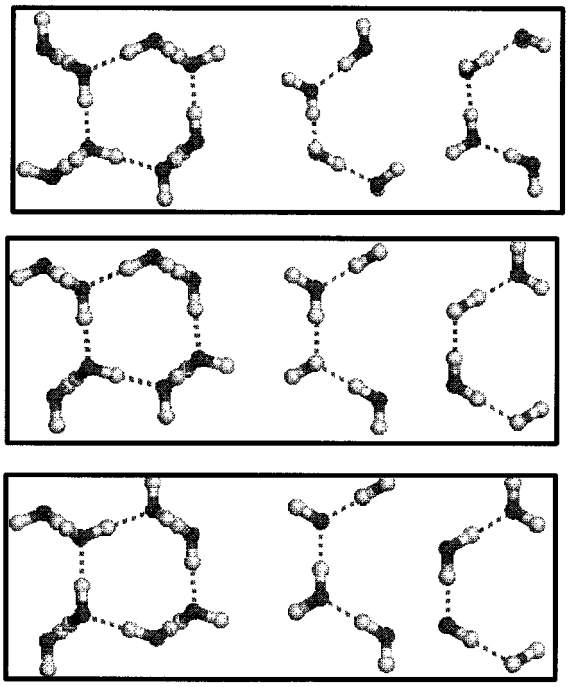

**Figure 2.** Three ordered ice Ih structures with eight-molecule unit cells (idealized model, no structural relaxation). Top: the antiferroelectric $Pna2_1$ structure. Middle: the ferroelectric $Cmc2_1$ structure. Bottom: the lowest energy structure found for the MKW model ($f_{trans} = 0.75$). Middle, right: projections of two hexagonal layers on the plane perpendicular to the *c*-axis. Left: "side view" on the unit cell, *c*-axis is vertical, shows orientation of eight molecules with respect to the c-axis.

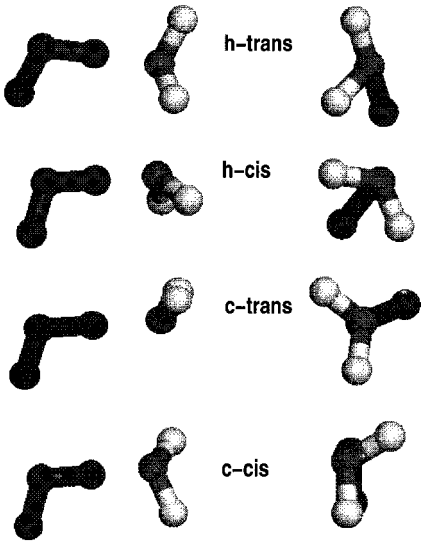


**Figure 3.** Four possible nearest neighbor configurations in ice Ih. Left/right projection on a plane parallel/perpendicular to the bond axis, respectively. Bottom two configurations: bond parallel to the *c*-axis. Top two configurations: bond nearly perpendicular to the *c*-axis. The dark and the bright hydrogens belong to the proton donor and proton acceptor, respectively.

H-atoms. In orientationally disordered ice, the statistical fraction of trans[16] is about 60%, while the proposed $Pna2_1$ structure is 100% trans.

However, recent neutron diffraction and thermally-stimulated depolarization studies[3] of ice XI (the ordered form of ice Ih obtained at 72 K) did *not* support the $Pna2_1$ structure. These data were interpreted in terms of the ferroelectric $Cmc2_1$ structure shown in Figure 2 (middle), which is only 25% trans. *So the question is what kind of water potential favors energetically a 25% trans structure with respect to the 60% disordered structure.* This question is addressed in the first part of this study, in section 2. The energies of different orientational structures (OCs) were calculated for six different "reasonable" water PES; however, we could not reproduce the required effect. We then identified a modification of the PES, which breaks the correlation between the percentage of trans pairs, and the crystal energy. A modified version of the polarizable potential of ref 5f is shown to yield lower energy for $Cmc2_1$ structure than for disordered ice, in accord with experiment. In section 3, this potential is further tested against ice, liquid, and cluster properties. In this part, various problems are discussed which are related to simulations of water and water clusters, and to comparison of theory and experiment.

One may question finally the usefulness of this study and of other efforts directed towards constructing a water PES, in view of current developments of "on the flight" dynamics. The latter does not employ analytical potentials at all; rather, the intermolecular interaction is calculated by solving the electronic Schroedinger equation at each simulation step.[17] The accuracy of "on the flight" potentials appears to be still well below that of the best analytical potentials; however, much effort is currently devoted to devising an optimal set of numerical parameters and procedures, adequate for DFT treatment of the hydrogen bonding. In some problems e.g., the ones involving ionization and chemical change, "on the flight" dynamics is most likely the method of the future. On the other hand, we believe that analytical water potentials are likely to be useful for quite a while in problems involving small energy differences (e.g., comparison of energetics of different ice[4b,5f,11] and ice surface[19] forms and of cluster isomers[5o,7d,20,21]), in lengthy molecular dynamics simulations of large systems (e.g., studies of dielectric properties[22] and of biomolecular solvation[23]), and in quantum mechanical studies of $H_2O$ nuclear dynamics.[4b,10,20,24,25]

## 2. Orientational Order−Disorder Transition in Ice: Energies of Different Orientational Configurations

**Synopsis.** We now focus on calculations of hexagonal ice energetics for different ordered and disordered H-atom arrangements. The question to be addressed is how different features of the potential affect the energy ordering of the configurations, and in particular, which features of the PES stabilize the observed low temperature ferroelectric $Cmc2_1$ ice structure[3] with respect to disordered ice. A new algorithm is presented for generating orientational configurations for ice Ih, obeying the correct ice rules. Then the nontrivial problem of obtaining accurate energies is discussed.

Initially, results are discussed for an idealized ice model, in which all O-atoms occupy periodic lattice sites, and H-atoms lie on nearest-neighbor O···O axes; energy differences between configurations are due to Coulombic interactions between atomic point charges. In this model, the energy decreases linearly with the fraction of nearest neighbor trans pairs $f_{trans}$ (see Figure 3). Therefore, the energy of the ferroelectric $Cmc2_1$ structure (with $f_{trans} = 0.25$) is higher than the energy of disordered ice ($f_{trans} \approx 0.6$), in contradiction to experiment. Introduction of ions into the model does not alter substantially the situation.

Then the ice structures were allowed to relax, and more realistic potentials were used. Energy minimization breaks the linear correlation between the energy and $f_{trans}$. However, for all literature potentials tested, the qualitative trend of energy decrease with $f_{trans}$ is retained, so that the required effect ($E_{Cmc2_1} < E_{disord}$) is not reproduced. We finally present a modification of the polarizable potential of ref 5f, which reproduces qualitatively the required effect. The correlation between the energy and $f_{trans}$ is broken by shifting the polarizability center on the water molecule by 0.48 Å away from the O-atom, along the water bisector. The modified potential is shown to yield reasonable energy and structure for disordered ice.

**2.1. Technical Details.** *2.1.1. Algorithm for Generation of Ice Structures.* A study of orientational energetics necessitated an algorithm for generation of a collection of ordered and disordered ice structures, all obeying the ice rules. The "disordered" ice models used in this study were periodic structures with large unit cells and with a disordered H-pattern inside the cells. Smaller unit cells were used to study ordered arrangements. The algorithm proposed here has the advantage of being automated and easy to program; for other approaches to generate ice structures, see refs 15 and 26. Initially, idealized ice structures were generated, in which all O···O nn distances were assumed equal to 2.75 Å and all O···O···O angles—perfectly tetrahedral. Moreover, H-atoms were placed on the O···O nn axes, 1 Å from these O atoms to which they are chemically bonded (i.e., the HOH molecular angle was also assumed perfectly tetrahedral.)

To obtain such structures, the following procedure was devised: (a) A rectangular unit cell of a desired size was programmed for the O-atoms (see Figures 1 and 2), using the well-known periodic O-atom arrangement.[1] (b) An H atom on each O···O nn axis was assigned at random one of the two allowed sites, 1 Å from one of the O atoms. At this stage, O-atoms may be "chemically bonded" to anywhere between zero and four H-atoms. (c) A Monte Carlo (MC) procedure was then applied towards correcting the initial H configuration, so

that eventually each O-atom is chemically bonded to exactly two H-atoms. In each MC step, a nn O···O axis was picked at random from the unit cell. The chemical coordinations of the two nn O-atoms are denoted $c_i$ and $c_j$, respectively. Reassignment of the H-atom on this O···O axis is then attempted from its current site to the alternative second site. The step is accepted with probability 1, if the result is the decrease of the coordination difference $|c_i - c_j|$; if no change in $|c_i - c_j|$ occurs, then the acceptance probability is $^1/_2$; otherwise, the step is rejected. The procedure is continued until $c_i = 2$ for all O-atoms.

Using this algorithm, ice Ih and Ic models were generated, containing up to 1600 water molecules. (Cubic ice Ic is a metastable form of ice characterized, similarly to ice Ih, by a nearly perfect tetrahedral hydrogen bond network, and orientational disorder[1]). The water bond lengths and angles were then readjusted to monomer geometries used in the different water PES. Particular attention was devoted to structures with eight molecules in a unit cell, with O-atoms arranged as in Figure 2. Using the above Monte Carlo procedure, we found 16 such distinct structures (using as distinctness criterion the value of the energy and of the dipole per unit cell, and the number of the different nn pair configurations, see Figure 3). In these 16 structures, the fraction of trans nn pairs $f_{trans}$ covers the range from 0 to 1, and the corresponding dipole moment per unit cell $M_0$ ranges from 0.9129 to 0. ($M_0$ is defined for the idealized unit cell as $M_0 = (\sum_{i=1}^{8} u_i)/8$, where $u_i$ is a unit vector along the bisector of molecule $i$). This set of configurations[27] includes the widely discussed $Pna2_1$ structure with $f_{trans} = 1$, $M_0 = 0$, and the ferroelectric $Cmc2_1$ structure with $f_{trans} = 0.25$, $M_0 = 0.577$ directed along the $c$-axis. Further discussion of these structures can be found in section 2.2.3; see also Table A1 in Supporting Information.

*2.1.2. Calculation of Energies of Different Orientational Configurations (OCs).* It should be noted in advance that calculation of OC energies is a computationally nontrivial task. Using the relation $\Delta U = T\Delta S$ for the orientational order−disorder transition at 72 K, and setting[1b] $\Delta S = 0.81$ cal/(mol K) for the ordered portions of ice, the orientational transition $\Delta U$ is 0.06 kcal/mol. Considering that the lattice energy of ice Ih at the minimum has been estimated as 14.1 kcal/mol,[28] the accuracy of the energy calculation must be better than 0.4%. Moreover (as explained in more detail below), electrostatic interactions between water molecules converge slowly as a function of distance, and careful treatment is needed of long range forces.

General Energy Formulas. The energy of the system is defined here as mean potential energy per molecule in a unit cell, where half of each interaction term between a pair of molecules $i$ and $j$ is assigned to $i$ and to $j$, respectively. Periodic boundary conditions enable use of potential cutoff larger than half the shortest dimension of the unit cell. The longest range intermolecular interaction term is dipole−dipole. This contribution converges for a sufficiently large cutoff distance. However, for unit cells with a net dipole, the energy of a ferroelectric crystal is dependent on the assumed macroscopic shape.[29,30] This is because surface charges due to the dipoles generate a shape dependent macroscopic field within the system, which interacts with the interior charge distribution. For an ellipsoid sample, the contribution to the total energy due to the interaction of an interior unit cell with surface charges is

$$V_\mu = (1/2v_o)\,[N_x(\sum\mu_{ix})^2 + N_y(\sum\mu_{iy})^2 + N_z(\sum\mu_{iz})^2] \quad (1)$$

where $v_o$ is the volume of the unit cell, the sums are over dipole components of all molecules within the unit cell, and the so called depolarization factors[29] $N_i$ are determined by the ratios of the principal axes of the ellipsoid. For a sphere, $N_i = 4\pi/3$. This contribution to energy is eliminated by metallic boundary conditions (immersion in a conductor).[14a,29] In natural ferroelectric crystals, the macroscopic electric field is mutually canceled by differently oriented ferroelectric domains.[29] In the present study, metallic boundary conditions are assumed (i.e., the macroscopic field is set to zero). Thus for pair-additive potentials, the mean intermolecular potential energy is calculated as

$$\bar{V} = [\sum_{i=1}^{N}\sum_{j} 0.5\, V_{ij} - V_\mu]/N \quad (2)$$

where $N$ is the number of molecules within a unit cell, the first sum (over $i$) is over all molecules in a unit cell, and the second sum is over interactions of each molecule $i$ with all molecules $j$ within a cutoff distance $r_c$ (the cutoff is defined for the O···O distance $|r_{oi} - r_{oj}| < r_c$).

For polarizable potentials, we employ procedures described (e.g., in ref 5b) and adjusted to the problem at hand. In these PES, induced molecular dipoles are calculated self-consistently. The electric field at a polarizability center on molecule $i$ is calculated by summing contributions from charges and induced dipoles within the cutoff; after which the macroscopic contribution due to the surface charges is subtracted from the field (the latter correction to the $k$th component of the field is equal to $N_k[\sum_i^N \mu_{ik}]/v_o$, $k = x, y, z$). The induced dipoles are iterated until convergence in potential energy is achieved. The electrostatic contribution to the PES is given by $\bar{V}_{el} = N^{-1}[V_{qq} + V_{qp} + V_{pp} + V_{self} - V_\mu]$ where $q$ denotes permanent charges; $p$, induced dipoles; and $V_{self}$ is the energy needed for creating the dipoles; the expressions for these terms can be found in ref 5b.

Some calculations were carried out with a simple flexible extension of the rigid PES, in which the following intramolecular term was added to the potential

$$V_{intra} = \sum_{m=oh1,oh2,hh} 0.5k_m(r_m - r_m^0)^2 + k'(r_{hh} - r_{hh}^0)(r_{oh1} + r_{oh2} - r_{oh1}^0 - r_{oh2}^0)$$

with "equilibrium distances" $r_m^0$ adopted from the monomer geometry of the corresponding rigid PES. The force constants are $k_{oh} = 0.5924$ au, $k_{hh} = 0.1317$ au, and $k' = -0.12$ au (the coupling term between the OH and the HH stretch was introduced to prevent decrease in the monomer angle upon structural relaxation, contrary to experiment).

Potential Minimization. The potential $\bar{V}$ was minimized with respect to the unit cell structure. The starting point for the minimization was an idealized structure (see section 2.1.1), with molecular geometry readjusted to the PES used. The minimization of the energy[31] was carried out with respect to the coordinates of molecules within the unit cell, and with respect to the unit cell dimensions. A potential cutoff of 60 Å was employed in the calculations. Additional information on the procedure (especially on the treatment of the cutoff which required some attention) can be found in Appendix I (see Supporting Information).

Energetics of Idealized Ice Ih: This simple ice model (see section 2.1.1) received special attention, as a starting point for more realistic calculations. It is used here in conjunction with the simple pair-additive SPC potential[4d] which is consistent with the idealized picture; in SPC, the HOH angle is tetrahedral, the

$H_2O\cdots H_2O$ interaction is composed of a Lennard-Jones term, centered on the O-atoms, and a Coulombic interaction between point charges placed on the three water atoms. The energy differences between different OCs are then due solely to Coulombic terms involving H-atoms. Based on this fact, one can simplify and expedite the energy calculation, as follows. For each OC, we imagine a "reference" configuration in which H-atoms are displaced to the middle of each nn O···O axis, and the point charges are rescaled so as to retain the dipole of water in the SPC model. All reference configurations have exactly the same potential energy, except for the surface charge contribution which is eliminated by metallic boundary conditions. The potential of a given OC is then calculated relative to the reference potential as

$$\bar{V} = N^{-1}\left[\sum_{i,j}(V_{ij} - V_{\mathrm{ref},ij})\right] \qquad (3)$$

where the sum is over the difference between the "true" Coulombic SPC interaction between a pair of water molecules, and the same interaction in the reference configuration. The surface charge contribution is removed automatically in this procedure, and the radius of convergence is much smaller (~13 Å) than using eq 2. It was verified that the two methods give the same results.

Simulation of Ice with Embedded Ions. It has been asked in the past whether the energetics of the orientational ordering transition is affected by the KOH impurity, which catalyses the transition. We attempted to address the possible role of KOH, by simulating a sphere of idealized SPC ice of 80 Å diameter, with a pair of +e/−e ions embedded in it at a distance of 41 Å from each other. The ions replaced two water molecules at the O lattice sites; the distance vector between the ions was along the *c*-axis. The initial H-atom distribution was disordered, except for the vicinity of the ions; a coordination shell of 4/0 hydrogen bonds was assigned permanently to the −e/+e ions, respectively. Monte Carlo simulation of the orientational energetics of the ice sphere with ions was carried out, using a straightforward adaptation to spherical geometry of a scheme described in ref 15. (To avoid spurious electric fields due to boundaries, the sphere was imagined embedded in a "very large" volume of reference ice.) The energy of the system is defined as in eq 3, with the addition of terms due to ion−water interactions. To accelerate the simulation, the temperature was rescaled gradually from 70 to 0.5 K. Further details can be found in Appendix II (see Supporting Information).

**2.2. Results: Orientational Energetics of Ice.** *2.2.1. "Idealized" Ice Ih. Here we imagine an idealized structure with O-atoms at periodic lattice sites, and H atoms on O···O nearest neighbor axes. As we shall see, this model is not very realistic, but it provides interesting insights for further discussion of more realistic models.*

As seen in Figure 4 (top), the orientational energetics in the idealized ice Ih and Ic model is rather simple. To a good approximation, the energy is determined by only one parameter of the structure, the fraction of trans nearest neighbor configurations $f_{\mathrm{trans}}$ (see Figure 3). That is, $\bar{V}$ decreases linearly with $f_{\mathrm{trans}}$, irrespective of the size of the unit cell, and the detailed orientational arrangement of the molecules. (We did not succeed in deriving analytically the linear dependence of $\bar{V}$ on $f_{\mathrm{trans}}$.) At a first glance, this simple result appears trivial, since trans nn configuration is substantially lower in energy than cis, due to reduced electrostatic repulsion. However, this physical interpretation is incorrect, because it disregards the long range of electrostatic interactions in the system. This point is

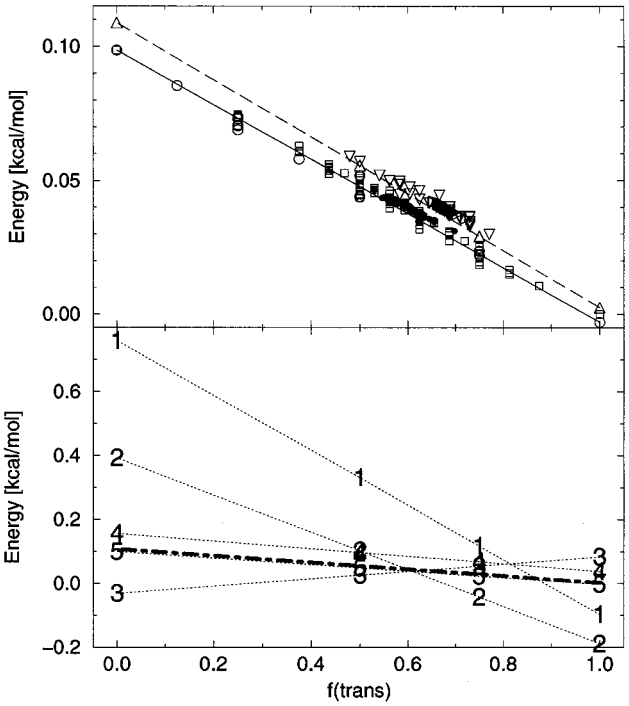


**Figure 4.** The energy $\bar{V}$ of different orientational configurations of idealized ice Ih and Ic, calculated according to eq 3, as a function of the fraction of trans nearest neighbor pairs. Top: $\bar{V}$ of ice Ih (circles, squares) and ice Ic (triangles). Number of $H_2O$ in unit cells: (circle) 8, (square) 16, (filled circle) 96, 360 and 1600, (triangle up) 8, (triangle down) 24, (triangle right) 512. The solid line for ice Ih and the dashed line for ice Ic were added to guide the eye. Bottom: The energy $\bar{V}$, of 4 different cubic ice configurations with a cubic eight-molecule unit cell, calculated with potential cutoffs 2.9, 4.7, 6.6, 7.1, and 13 Å (graphs 1−5), and 60 Å (dot−dashed). Graphs 1-4 include first, second, fourth, and fifth nearest neighbor interactions, respectively. Zero of the energy was set slightly above $Pna2_1$ energy ($\bar{V}_{\mathrm{Pna2_1}} = -0.0029$ kcal/mol).

demonstrated in Figure 4 (bottom), which shows the energy of four different cubic ice configurations with a cubic 8 molecule unit cell, and $f_{\mathrm{trans}}$ ranging from 0 to 1. $\bar{V}$, calculated according to eq 3, is shown for several potential cutoffs. If only nearest neighbor interaction is included (graph 1), then, of course, the 100% trans configuration is by far most stable. However the interactions are long ranged, and there is much cancelation e.g., if four nearest neighbor interactions are included (graph 3), then the energy ordering is *reversed*, and the 100% cis configuration becomes most favorable. Inclusion of 5th nearest neighbors (graph 4), reverses again the energy ordering, and the energy values are converged finally for a cutoff near 13 Å.

Definition of energy of a disordered model requires some care, since there is a very large number of such structures. However as the size of the unit cell increases, the energy range of structures generated by our Monte Carlo procedure decreases and approaches a limit. One may compare results obtained for a 96-molecule and a 1600-molecule unit cell (30 and 10 different configurations, respectively). Mean energy, calculated with eq 3 is 0.0394 and 0.0396 kcal/mol/molecule for the two sizes, with standard deviations of 0.0035 and 0.0006 kcal/mol/molecule, respectively. The mean value of $f_{\mathrm{trans}}$ is 0.604 and 0.602, with standard deviations of 0.037 and 0.008, respectively. It seems not unreasonable to assume, that our procedure generates "typical" disordered configurations whose properties can be used for studies of disordered ice.

Using $\Delta S = 0.81$ cal/(mol K), and the energy difference between the lowest energy $Pna2_1$ structure ($f_{\mathrm{trans}} = 1$) and the mean energy of the largest disordered model with 1600

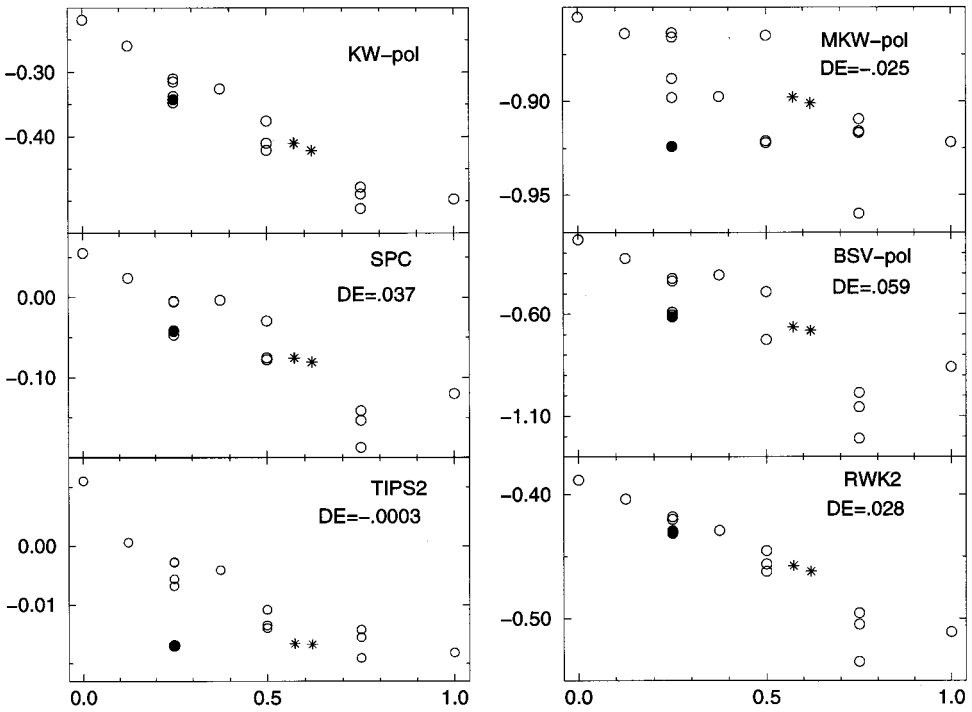


**Figure 5.** Minimum potential energies $\bar{V}_{min}$ of various orientational configurations, as a function of the fraction of trans nearest neighbor pairs, for various water potentials (see section 2.2.3). Circles: OCs with an eight-molecule unit cell. Filled circle: $Cmc2_1$ configuration. Stars: Two disordered models with a 96-molecule unit cell. Zero of the energy was set at −13.4483 kcal/mol.

molecules, we obtain orientational transition temperature of 52 K. A similar result was obtained in ref 15, in a Monte Carlo simulation of the order−disorder transition starting from the $Pna2_1$ structure, and employing a related idealized model. This temperature is in reasonable agreement with the experimental value of 72 K; however, the ordered $Pna2_1$ structure is not in accord with experiment.[3] In the idealized model, the energy of the experimental $Cmc2_1$ structure is *above* the mean disordered one. *Thus, the idealized ice model is inadequate for explaining the 72 K transition to the ordered* $Cmc2_1$ *ice structure.*

*2.2.2. Possible role of KOH impurity?* It has been questioned in the past (see, e.g., ref 15) whether the 72 K transition is intrinsic to ice. The transition has been demonstrated in the presence of KOH impurity, and the question is whether the sole role of the impurity is to keep the molecules orientationally mobile down to 72 K, or whether in addition KOH alters the energetics by stabilizing the $Cmc2_1$ structure. At a first glance, this does not seem likely; one would think that an ionic impurity would induce some structural modification which decays radially as a function of distance, rather than a transition to a periodic crystalline structure with an orthorhombic unit cell. But this point is far from clear.

We addressed the possible role of KOH in a limited fashion, using a Monte Carlo simulation of orientational energetics in a sphere of idealized SPC ice, with a pair of +e/−e ions embedded in it, as described in the end of section 2.1.2, and in Appendix II. *The qualitative question was whether the presence of ions stabilizes a cis-rich structure, and/or induces a dipole along the c-direction. The result was negative.* The presence of ions did not result in increased percentage of cis pairs in the system, with respect to disordered ice; rather, $f_{trans}$ increased during the simulation from 0.6 to 0.9. No significant increase in the sphere dipole was obtained in the two simulations, with respect to the initial state (corresponding to two ions in disordered ice).

*2.2.3. Minimum Energies of Orientational Configurations for Different Water Potentials.* The idealized ice model suffers from many deficiencies. For example, the ordered ice structure undergoes structural relaxation with respect to the idealized ice Ih structure, and relaxation should affect the relative energies of the different OCs. Also, the simple SPC potential may be inadequate (e.g., it does not include non-pair-additive interactions, or anisotropy of the repulsive core). *In this part, we consider energies of various orientationally ordered and disordered ice models (without ions), for a variety of pair-additive and polarizable water potentials.* The energies are calculated for *relaxed* (i.e., minimized) unit cell structures. Our aim is to assess how different features of the PES affect the orientational energetics. We note in advance that none of the potentials yielded $Cmc2_1$ as the lowest energy configuration. However, experimental data do not necessarily indicate $Cmc2_1$ as the *ground state*, since the 72 K phase transition could conceivably occur to a metastable ordered state. Still, we expect the "correct" PES to yield $Cmc2_1$ energy which is lower than energy of the disordered structures. An effort was made to find a PES which satisfies this condition.

The calculations were carried out for various ordered OCs with an 8-molecule unit cell, and also for two disordered structures with a 96-molecule unit cell (see section 2.1.1, and Figures 1 and 2). In the idealized model, the two disordered structures have energies of 0.0378 and 0.0427 kcal/mol/molecule (the mean value is 0.0394 ± 0.0035, see section 2.2.1). The relative smallness of the "disordered" unit cell is due to a large amount of computer time needed for the minimization. However, the idealized model suggests that a 96-molecule cell provides a reasonable representation of properties of much larger disordered cells (see section 2.1.1). It is assumed that the same holds true after the minimization. We are encouraged by the fact that the two disordered structures remain energetically close after the minimizations (see Figure 5).

The calculations employed a number of popular pair-additive potentials (SPC,[4d] TIPS2, TIP4P,[4c] RWK2[4b]), and two polarizable potentials, denoted here by BSV[5m] and KW[5f] (the authors' initials of refs 5m and 5f), which were parameterized specifically

**TABLE 1: Factors by Which Orthorombic Unit Vectors of $Cmc2_1$ Ice Differ from Corresponding Vectors for O-Arrangement in Disordered Ice[a]**

| PES | $f_x$ | $f_y$ | $f_z$ |
|---|---|---|---|
| exptl[3b] | .993 | 1.009 | .996 |
| SPC[4d] | 1.052 | .955 | .992 |
| TIPS2[4c] | 1.010 | .982 | 1.007 |
| RWK2[4b] | .983 | 1.016 | 1.003 |
| BSV[5m] | 1.115 | .901 | .967 |
| KW[5f] | 1.030 | .977 | .995 |
| MKW | 1.013 | .988 | .997 |

[a] Three numbers refer, respectively, to the horizontal, vertical, and "into the page" directions of unit vectors in Figure 2, top-right.

in the context of solid $H_2O$. Figure 5 shows minimum energies $\bar{V}_{\min}$ for various OCs. The results for TIP4P are not displayed, since they are qualitatively similar to TIPS2. Note the different energy scales for different potentials, and the values of DE = $\bar{V}_{\mathrm{Cmc2_1}} - \bar{V}_{\mathrm{disord}}$ (the difference between the energy of the $Cmc2_1$ structure, and the mean energy of the two disordered models). For comparison, the experimental $\Delta U$ between the ordered and the disordered structure is about $-0.06$ kcal/mol. Another piece of pertinent experimental data pertains to the difference between the unit cell dimensions in orientationally ordered and disordered ice; experimental results and calculations are compared in Table 1.

We first discuss the five PES other than the one marked MKW. SPC[4d] corresponds to the simplest "zero-order" model, which includes a Lennard-Jones function of the O···O distance, and Coulombic interactions between three point charges located on the water atoms. However, it has been often argued that the description of water potential can be improved by shifting the negative charge from the O-atom down the water bisector, toward the H-atoms.[4,5] In this way, improved representation is obtained of the water quadrupole, and since hydrogen bonding is electrostatic in nature, better representation of monomer electrostatic properties seems advantageous. All PES included in Figure 5 other than SPC correspond to a shifted negative charge. In particular, TIPS2[4c] is a simple pair-additive potential similar to SPC, the main difference being the negative charge shift. RWK2[4b] was constructed in an effort to reproduce reasonably properties of the different water phases—vapor, liquid, and three forms of crystalline ice, in the framework of a pair-additive PES. The new feature of RWK2 is a more elaborate treatment of the repulsive core, which is represented by several exponentially repulsive and Morse terms centered on the water atoms. A simple polarizable potential BS[5m] includes three point charges, a single dipole polarizability center placed at the center of mass, and O···O Lennard-Jones interaction which was parameterized to reproduce ice Ih lattice energy and O···O distance. Finally, the polarizable KW potential[5f] differs from BSV by more elaborate parameterization of the anisotropic repulsive core (represented by exponentially repulsive interatomic terms), and by introduction of shielding of the electric field induced by the charges at the point polarizability site (the O-atom). At short distances point charge/point polarizability description breaks down, resulting in artificially large induced dipoles; and distance dependent shielding is a practical invention to avoid this artifact. The repulsive core was parameterized against ab initio data on the water dimer. The shielding was found unimportant for the dimer, but necessary for representing properties of the three ordered forms of ice discussed in ref 5f.

The corresponding orientational energetics is displayed in Figure 5. The energy span of different OCs ranges from only 0.03 kcal/mol for TIPS2, to about 1 kcal/mol for the polarizable BSV. However, the results for the five different PES have some crucial features in common. It is seen that structural relaxation and other changes with respect to the idealized model disrupt linear correlation between $f_{\mathrm{trans}}$ and the energy. For example, after inclusion of the relaxation, the lowest energy configuration is no longer the $Pna2_1$ with $f_{\mathrm{trans}} = 1$, but rather a zero-dipole structure with $f_{\mathrm{trans}} = 0.75$. *Still, the general trend of energy decrease with $f_{\mathrm{trans}}$ is retained to a sufficient degree to make the disordered structures with $f_{\mathrm{trans}}$ near 0.6 lower in energy than the $Cmc2_1$ structure with $f_{\mathrm{trans}} = 0.25$, in contradiction to experiment.* The exception is the TIPS2 potential, for which the disordered structures are nearly isoenergetic with both $Pna2_1$ and $Cmc2_1$.

The calculated differences in unit cell dimensions between disordered ice and $Cmc2_1$ are generally too large (see Table 1). RWK2 is the only potential that yields $f_x < f_y$, in qualitative accord with experiment. It is instructive to note the nonsensical results obtained with the simple polarizable BSV potential, for which two of the $Cmc2_1$ lattice unit vectors differ by ~10% with respect to disordered ice, while the experimentally observed differences are less than 1%. This result underscores the need for careful treatment of the repulsive core in a polarizable PES. Ice properties represent delicate balance between the repulsive core and the electrostatic forces, and thus are particularly sensitive to the repulsive core shape (probably much more so than the liquid). In polarizable potentials, induced dipoles result in strong attractive forces at short distances, and therefore, deficiencies in repulsive core treatment are particularly apparent (see also refs 5i and 5o on this matter).

Modified KW (MKW) potential represents our effort to readjust the polarizable KW potential, to obtain lowering of the $Cmc2_1$ energy with respect to the disordered ice. We were searching for that modification of the PES that will disrupt the correlation between $\bar{V}$ and $f_{\mathrm{trans}}$, while retaining a reasonable description of other properties. Disruption of correlation could be achieved by shifting the polarizability center away from the O-atom, down the bisector toward the H-atoms. Shift by 0.283 Å, to the site of the negative charge, reduced DE from 0.08 to 0.02 kcal/mol. Negative DE ($-0.016$) was obtained by using a shift of 0.48 Å for the polarizability, together with reduction of the shielding range parameter ($r_s$ of ref 5f) from 1.45 to 1.25, and change of the exponential repulsion parameter $b_{oo}$ from 2.6975 to 2.65. This modified KW potential is denoted henceforth MKW. The flexible version of MKW (see section 2.1.2 above) resulted in DE = $-0.025$ kcal/mol. The size of this DE is too small (the "experimental" value is $-0.06$ kcal/mol), but at least the sign and the order of magnitude is correct, in contrast to all other PES examined. Also, as seen in Table 1, the MKW values of $f_x$, $f_y$, $f_z$ are closer to experimental than the values for all other PES except for the nonpolarizable RWK2 (which yielded a wrong sign for DE). Examination of Figure 5 confirms extensive disruption of the correlation between $\bar{V}$ and $f_{\mathrm{trans}}$ for MKW, as compared to all other PES. More detailed information on the energy components of the different minimum energy structures in the MKW potential, and their dipole moments, is given in Table AI (see Supporting Information). One may note that the $Cmc2_1$ structure is the second lowest structure found. The lowest energy structure corresponds to $f_{\mathrm{trans}} = 0.75$ and zero global dipole, and is shown in the bottom of Figure 2. It is stabilized with respect to other structures by a particularly large negative component of interactions involving the induced dipoles (see Table AI).

It should be noted that the optimal representation of polarizability on the water molecules is far from clear. A number

**TABLE 2: Properties of Ice Ih: Calculations with MKW Potential versus Values Derived or Estimated from Experiment[d]**

| property | experimental | calculated | units |
|---|---|---|---|
| minimum energy | 14.1[a] | 13.8,[d] 14.3[e] | kcal/mol |
| mean molecular dipole | 2.45,3.00[a,b] | 2.81,[d] 2.90[e] | debye |
| mean equilibrium OH bond length | 0.973[c] | 0.984[e] | angstroms |
| mean HOH angle | 107[c] | 105[e] | degrees |

[a] Reference 28. [b] Two different estimates. [c] Reference 32. [d] Values pertain to the rigid version of MKW. [e] Values pertain to the flexible version of MKW.

of models introduced three polarizability centers on (or in the vicinity of) the three water atoms (see, e.g., refs 5c, 5k, 5l). Many past studies employing a single polarizability center set it on the O-atom, or nearby on the $H_2O$ center of mass; however, the main reason seemed to be computational convenience. In the NCC potential of ref 5h, two polarizability centers were set on OH bonds, 0.433 Å from the O-atom. In ref 5o, a single polarizability center coincides with the location of the negative charge, shifted 0.215 Å down the bisector. The present study suggests that orientational energetics is a particularly sensitive constraint for the representation of the polarizability.

Since the proposed location of the polarizability center in MKW is somewhat unconventional, we proceeded to test it on other (disordered) ice properties. The MKW unit cell vectors are overestimated by 1% with respect to the experimental values given in ref 3b. Four additional properties are given in Table 2, the agreement is not unreasonable.

## 3. Simulations of Liquid $H_2O$ and of Water Clusters

**Synopsis.** In the previous section, we have tested water PES for a property which seems particularly hard to reproduce: how to make the experimentally observed ordered ferroelectric form of ice Ih, $Cmc2_1$, more stable than disordered ice. This effect was reproduced qualitatively, using a modified version of the polarizable KW potential[5f] (MKW). It is clear that further improvements of the PES are possible, but were not attempted in the present study. Instead, we proceed to test the performance of MKW as a relatively simple "minimalistic" polarizable PES for modeling of $H_2O$, with the hope for a reasonably balanced description of a broad range of $H_2O$ behaviors.

In this section, MKW is tested on $H_2O$ liquid and cluster properties (most notably, on the recently available rotational constants[7] of $(H_2O)_n$, $n = 3-6$). The more philosophical question is the following: How well can one do with a relatively simple polarizable PES, which was *not* parameterized against these data? In this context, certain technical problems are discussed, which are related to the pertinent simulation techniques and to comparison between theory and experiment.

In the case of the liquid (which was simulated by classical molecular dynamics), MKW is shown to perform quite well for the self-diffusion constant, the dielectric constant, and the peak positions of the radial distribution functions (rdfs). The peak heights are however overestimated with respect to rdfs derived from the latest neutron diffraction data. At least some of the overestimation is due to the use of classical mechanics. (One may note however that the peak heights are the least well determined feature of the experimental rdfs.)

The clusters were simulated using rigid body diffusion Monte Carlo (RBDMC[33,34]). Solutions were suggested to some nontrivial technical problems associated with calculations of rotational constants averaged over the zero-point motion. The experimental rotational constants for the cyclic $n = 3-5$ clusters and for the $n = 6$ cage are reproduced very well (within several tens MHz) in the framework of the MKW potential. The results for the dimer are less satisfactory; the rotational constant $B_0$ is too large by a few hundred MHz, and the well depth is overestimated by some 8% with respect to the best ab initio results.

A very stringent test of the potential in the context of cluster studies is the ability to predict energy ordering of different (numerous) isomers, for $n \geq 6$. Experimentally, at $n = 6$ a transition occurs from a cyclic to a three-dimensional (3D) cluster structure.[7d,9a] For $n = 7$, MKW yields a clear preference for a three-dimensional structure, while for $n = 6$ the binding energies of a cyclic structure and of the experimentally observed 3D "cage" are nearly equal. After the zero-point energy correction, the cage is less stable than the hexamer cycle by 0.5 kcal/mol (170 $cm^{-1}$); errors in the PES of this size are not unexpected. Thus, MKW is insufficiently accurate to *predict* energy ordering of cluster isomers on this level of accuracy (the same is probably true for other currently available ab initio and empirical potentials.) Still, MKW seems useful for producing candidate cluster structures of low energies; the final assignment of the observed species can be then made by comparing calculations to measured properties, such as rotational constants or OH- stretch spectra. (MKW potential has been recently used in this way for the assignment of the nonamer and decamer structures.[10])

**3.1. Molecular dynamics simulations of liquid $H_2O$.** Rigid body MKW potential was used throughout the remainder of this paper, unless otherwise stated. The details of the 1.15 nanosecond classical trajectory NVE simulation[23,35] ($\bar{T} = 296$ K) are given in Appendix III (see Supporting Information). Calculations of the dielectric constant require special care in treatment of long range forces.[36] Here, we employed the reaction field method,[22,36,37] which treats the material beyond the cutoff sphere ($r_c = 9$ Å) as a polarizable continuum, exerting a reaction field at the central molecule. The method was criticized in the past for assuming instantaneous response of the reaction field to the dipole of the cutoff sphere. However, as explained in Appendix III, the discussion of ice in the previous section suggests another interpretation of the reaction field formulas, and supports their use. The reaction field correction can be viewed alternatively as cancellation of spurious torques on the central molecule, due to anisotropic charge distribution on the spherical boundary; these torques are canceled in reality by additional molecules beyond the cutoff.

*3.1.1. Results: Liquid Simulation.* The calculated self-diffusion coefficient, $2.4 \times 10^{-5}$ $cm^2$ $s^{-1}$, is in good agreement with the experimental 295 K value[38] of $2.3 \times 10^{-5}$ $cm^2$ $s^{-1}$. The difference between the calculated dielectric constant $\epsilon = 87$ and the experimental 298 K value[39] $\epsilon = 79$ is of order of the computational error (see Appendix III); for comparison, $\epsilon$ values reported for other potentials[22] are 54−73 (SPC), 62.3 and 71 (SPC/E), 83 (flexible SPC), 79 (TIP4P-FQ[5k]), 116 (SPC-FQ[5k]), and 63 (KW, present study, obtained from a 0.9 ns trajectory).

The comparison of the calculated mean intermolecular potential ($\bar{V} = -10.0$ kcal/mol) to the experiment is complicated by the fact that the present simulation is classical, and rigid body. The experimental $\Delta E$ of vaporization is 9.92 kcal/mol at 298 K and 1 atm.[4c] To obtain "experimental" $\bar{V}$, we correct this value for (a) the difference between the gas and the liquid intramolecular zero-point energy (−0.6 kcal/mol[40]); (b) the difference between the kinetic + rotational energy in the gas phase, and in the liquid, which according to quantum-mechanical

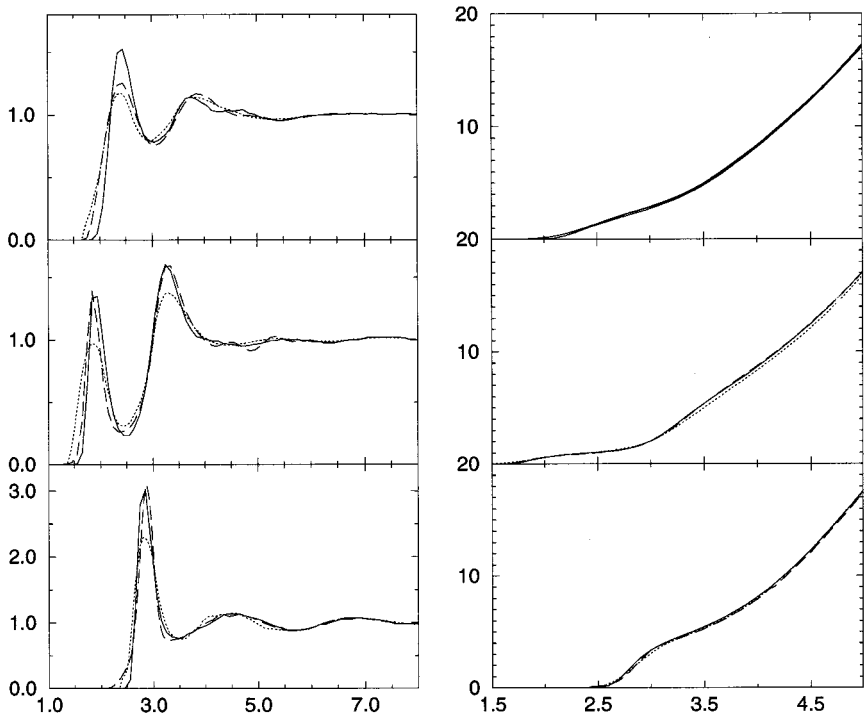


**Figure 6.** Calculated (solid line) versus experimental (dashed,[42a] dotted[42b]) radial distribution functions; from bottom to top: $g_{oo}$, $g_{oh}$, and $g_{hh}$, together with the corresponding integrated numbers of neighbors within a sphere of radius $r$.

path integral Monte Carlo (PIMC) simulations of water is 0.4−0.5 kcal/mol;[24a,b] (c) the energy needed to stretch OH bonds by about 0.01 Å (the difference between the bond lengths in the two phases[41]) ∼0.1 kcal/mol. The corrections cancel, and the resulting $\bar{V} = -9.92$ kcal/mol compares quite favorably with the calculated −10.0 kcal/mol. However, a quantum simulation of the liquid with the same potential would probably raise $\bar{V}$ by some 0.6−0.8 kcal/mol.[24]

Figure 6 shows the calculated versus experimental radial distribution functions (rdfs) $g_{oo}$, $g_{oh}$, and $g_{hh}$, together with the corresponding integrated numbers of neighbors within a sphere of radius $r$, which is $4\pi\rho\int_0^r g_{mn}(r)r^2\,dr$. The experimental rdfs are derived from neutron diffraction data. Two sets of experimental rdfs are given: the "classic" 1986 set[42a] which has been used extensively to test and calibrate water potentials[4,5]), and a 1997 set[42b] based on new data extending to higher $Q$ values. The new data are characterized by broader peaks, of lower peak intensities. The calculated rdfs agree much better with the old set than the new one; which is also true for other published potentials (that were largely parameterized against the older set), such as SPC,[4d,24a] TIPS2 and TIP4P,[4c] PSPC,[5b] TIP4P-FQ,[5k] and polarizable potentials of refs 5k, 5l, 5o. A reduced height of the first $g_{oo}$ peak (which is also in agreement with older X-ray data[42c]) was obtained for ab initio derived potential NCC,[5h] and in a DFT/BLYP "on the flight" molecular dynamics study of ref 17, while the peak heights of $g_{oh}$ obtained in both of these studies are still larger than the new experimental set. Some of the overestimate in peak heights in Figure 6 must be due to neglect of quantum effects, which, according to past PIMC studies of liquid wate[24] broaden the peaks; the resulting reduction in peak heights is in the range 0.1−0.3 units, and seems to depend on the potential used. One should note at this point that the neutron diffraction data measure best the peak locations, and the integrated rdfs, which are reproduced rather well in the present model (see Figure 6); while the "experimental" peak heights and widths are more uncertain, due to difficulties in obtaining reliable high $Q$ scattering data. The $g_{oo}$ is the least well defined since the OO contribution to the total neutron scattering pattern is only 10%.

**3.2. Simulations of water clusters $n \leq 7$.** Another stringent test of the potential is the ability to reproduce experimental data[6−10] on water clusters $(H_2O)_n$. Here we focus largely on shapes of the lowest energy cluster structures, as reflected experimentally by rotational constants,[6,7] and by OH-stretch spectra.[8−10] Modeling of floppy anharmonic hydrogen bonded clusters poses an interesting technical challenge. The number of potential minima increases rapidly with the cluster size. Moreover inclusion of quantum vibrational effects is necessary, since zero-point motion in the cold hydrogen rich clusters affects significantly energy ordering of structures and other measurable properties (as demonstrated elegantly for $n = 6$[7d]).

*3.2.1. Methods.* Cluster minima were calculated using the conjugate gradient algorithm,[31] with initial conditions corresponding to a water ring, or two water rings randomly displaced and rotated with respect to each other; in addition, "noise" was added to the center-of-mass $H_2O$ coordinates. Some of the minima are shown in Figure 7. The intermolecular zero-point motion was studied using the QCLUSTER program[43] based on the the RBDMC algorithm.[33,34] DMC is a numerical method to solve time independent Schroedinger equation by a random walk of a cloud of replicas of a quantum system;[33] in the long time limit, the distribution of replicas in space approaches the vibrational wave function Ψ. The rigid body DMC treatment developed in our group[34] reduces the problem of numerical noise, and allows for larger Monte Carlo steps; it is justified by the large gap between the inter- and intramolecular frequencies. The present calculations employed 2000 replicas, a time step of 30 au, and 5000∼15000 steps per simulation. RBDMC was used to obtain intermolecular contribution to zero-point energies, and to evaluate expectation values of rotational constants (RC), averaged over the vibrational zero-point motion.

RBDMC calculation of RCs is associated with some technical challenges, which are described in detail in the Appendix IV (in Supporting Information). The first problem is how to define

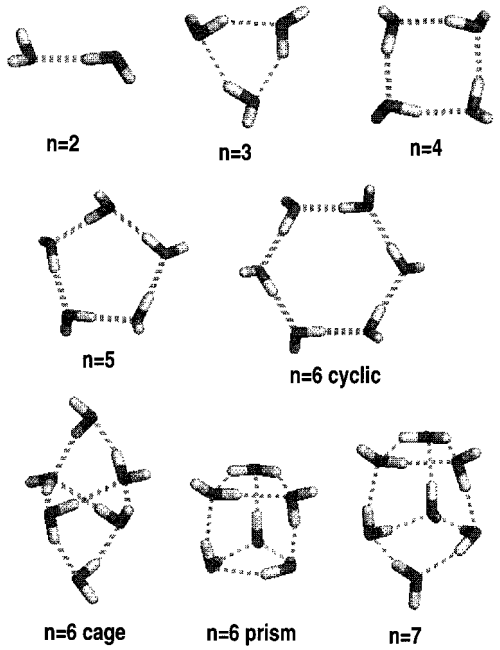


**Figure 7.** Minimum energy structures of water clusters $(H_2O)_n$ obtained with MKW potential.

the functions of coordinates whose expectation values yields the RCs. One possibility[20,34] is to evaluate *A*, *B*, and *C* constants for each replica, and then to average over the distribution. Another option is to implement a treatment of ref 44a, in which rotation is separated from vibration with the help of Eckart conditions.[34c,44] The latter treatment employs a rotating coordinate system attached to some reference cluster configuration (assumed planar and equilateral for the cyclic $n = 3-5$ clusters). Physically, in the first scheme a rotating cyclic cluster "sees" a "typical" irregular configuration, while in the second, a symmetric equilateral shape of sides equal to the mean $r_{oo}$ value. The second point of view seems closer to reality, since the observed far infrared bands were well fitted using symmetric rotor formulas with $A = B \sim 2C$.[7a-c] We then employed Eckart separation in all the calculations of Table 3. The second problem is that the DMC simulation generates a distribution mimicking $\Psi$ rather than $\Psi^2$. The computational trick used to obtain mean values of functions of coordinates (such as RCs) is then to perform the averaging over the replica distribution, while weighting a contribution of replica *i* by an extra factor $d_i$ that is proportional to $\Psi$. The well known descendent weighting (DW) method[33] to generate $d_i$ by counting descendents of replicas after some time delay is associated with numerical difficulties for the larger clusters (see Appendix IV). We then employed our alternative pair counting (PC[34c]) method, in which $d_i$ is set to the number of neighboring replicas found within some volume $V_i$ around replica *i*. Before determining $d_i$, the irrelevant degrees of freedom (global rotation and translation) were eliminated by overlapping the replicas, via minimization of mass weighted root mean square distance with respect to the reference configuration.[45]

The cluster energetics may be affected not only by intermolecular zero-point energy effects, but also by intramolecular ones, particularly the OH-stretch contribution. This is since the OH-bond frequency is red shifted by up to $\sim 800$ cm$^{-1}$ by hydrogen bonding with other water molecules. To estimate the intramolecular zero-point energy, we employed ideas from a recently devised treatment of OH stretch spectra.[10] The treatment relies on the results of past ab initio studies[46] which suggested that the OH-bond frequency $\omega_b$ is a function of calculated $E_{||}$, the electric field component along the OH bond, at the location of the H-atom. This function was calibrated by plotting the experimental frequencies for $n = 3-5$[8] and $n = 8$[10] as a function of $E_{||}$ at cluster minima. The OH contribution to zero-point energy is then estimated as a sum of the bond ground state energies (where OH-bonds are treated as Morse oscillators).

**TABLE 3: Rotational Constants of Water Clusters $(H_2O)_n$ in MHz, Calculated versus Experimental**

| *n* | | *A* | *B* | *C* |
|---|---|---|---|---|
| $(H_2O)_2$ | exptl[a] | | 6161[b] | |
| $(H_2O)_2$ | DMC/MKW[c,d] | | 6473[b] | |
| $(H_2O)_2$ | min/MKW[d,e] | | 6632[b] | |
| $(H_2O)_2$ | DMC/KW[c,f] | | 6626[b] | |
| $(D_2O)_2$ | exptl[a] | | 5432[b] | |
| $(D_2O)_2$ | DMC/MKW[c,d] | | 5808[b] | |
| $(D_2O)_2$ | min/MKW[d,e] | | 5795[b] | |
| $(D_2O)_3$ | exptl[g] | 5796 | 5796 | 3088 |
| $(D_2O)_3$ | DMC/MKW[c,d] | 5799 | 5747 | 2873 |
| $(D_2O)_3$ | min/MKW[d,e] | 5892 | 5798 | 3035 |
| $(D_2O)_4$ | exptl[h] | 3080 | 3080 | $1500 \pm 250$ |
| $(D_2O)_4$ | DMC/MKW[c,d] | 3097 | 3085 | 1540 |
| $(D_2O)_4$ | min/MKW[d,e] | 3056 | 3056 | 1589 |
| $(D_2O)_5$ | exptl[i] | 1751 | 1751 | ~875 |
| $(D_2O)_5$ | DMC/MKW[c,d] | 1769 | 1743 | 875 |
| $(D_2O)_5$ | min/MKW[d,e] | 1737 | 1715 | 888 |
| $(H_2O)_6$ | exptl[j] | 2164 | 1131 | 1069 |
| $(H_2O)_6$ | DMC/MKW[c,d,k] | 2174 | 1086 | 1029 |
| $(H_2O)_6$ | min/MKW[d,e,k] | 2248 | 1122 | 1091 |
| $(H_2O)_6$ | DMC/KW[c,f,k] | 2155 | 1095 | 1041 |
| $(H_2O)_7$ | DMC/MKW[c,d,l] | 1319 | 888 | 874 |
| $(H_2O)_7$ | min/MKW[c,e,l] | 1353 | 957 | 909 |

[a] Reference 6. [b] $B_0 = 0.5(B+C)$. [c] Rotational constants averaged using RBDMC with pair counting and Eckart separation, for more details see Appendix IV (Supporting Information). [d] MKW potential, see text. [e] Rotational constants at minimum configuration. [f] KW potential, reference 12. [g] Reference 7a. [h] Reference 7b. [i] Reference 7c. [j] Reference 7d. [k] Cage hexamer configuration. [l] Lowest MKW heptamer minimum.

A known problem with polarizable potentials is a possibility of induced dipole divergence at short distances. While we did not encounter it in liquid or ice simulations, it appeared occasionally for clusters, for large minimization steps. The problem was eliminated by setting the potential to a "very large" value for $r_{oo} < 2.1$ Å.

*3.2.2. Results: Cluster Rotational Constants (RCs).* The results are shown in Table 3, and compared to experiment.[6,7] The *A* and *B* rotational constants of the cyclic clusters $n = 3-5$, calculated by RBDMC with the MKW potential, are within a few tens MHz from each other and from the experimental values; note that the experimental data[7a-c] were fitted by symmetric rotor formulas with $A = B$. The hexamer cage RCs were also reproduced within a few tens MHz. For the $(H_2O)_2$ and $(D_2O)_2$ dimers, the agreement with experiment[6] is much poorer: the calculated $B_0$ is too large by 312 and 376 MHz, respectively. Thus, the MKW potential as a tool to extrapolate between gas phase and condensed phase properties does not perform that well at $n = 2$. MKW well depth of the dimer, $-5.476$ kcal/mol, also appears to be too large, since according to recent advanced ab initio calculations the correct value is 5.05 kcal/mol.[47] The RCs calculated at the minimum differ from RCs averaged over zero-point motion by up to 160 MHz, interestingly, the averaging may either lower or increase the RCs with respect to minimum values.

*3.2.3. Results: Structure and Energetics for $n = 6-7$.* It is known from experiment[8,9a] that at $n = 6$ a transition occurs from a cyclic to a three-dimensional water cluster structure. Theoretical studies employing various ab initio and empirical

potentials agree on presence of a number of different minimum energy hexamer structures of similar energies, but the energy ordering varies from method to method.[20,48] It is the belief of the present authors that none of the currently available theoretical methods is sufficiently accurate to *predict* reliably the energy ordering of closely spaced isomers for $n \geq 6$. However, calculations can be used to generate a collection of viable candidate structures, which can be then tested against experimental data. Comparison of calculated RCs to the experimental ones demonstrated[7d] presence of a three-dimensional cage structure for the hexamer. An RBDMC study[7d] employing a polarizable extension of the PES of ref 5g demonstrated an interesting quantum effect in which the cage, which does *not* correspond to the lowest energy minimum, becomes a lowest energy structure after addition of the intermolecular zero-point energy.

For $n = 6$, the present MKW potential yielded, similar to other studies, a large number of minima which can be divided to structurally related families. The lowest energy minimum located corresponded to a prism (two fused triangular cycles). The energies of the lowest prism/cage/cyclic minima shown in Figure 7 are −46.27/−45.49/−43.93 kcal/mol, respectively; however, after the inclusion of intermolecular zero-point contribution, the energy ordering is reversed: −30.60/−30.83/−31.17 kcal/mol (the error due to numerical noise is up to ∼0.06 kcal/mol). The dramatic effect of zero-point energy is related to the fact that in prism all water molecules are 3-coordinated, in the cycle all are 2-coordinated, and in the cage the number of 2- and 3-coordinated is 2 and 4, respectively (see Figure 7). Molecules of higher coordination are associated with less freedom of motion, and thus higher zero-point energy. In MKW, the cycle is more stable than cage by a total of 0.5 kcal/mol (170 $cm^{-1}$), after inclusion of the zero-point intramolecular contribution; in assessing these numbers one should note that this difference is ∼1% of the minimum energy.

For the heptamer, MKW yields a lowest energy three-dimensional minimum shown in Figure 7 which is now clearly more stable than the cyclic form (by 2.7 kcal/mol, including the zero-point energy correction). The structure looks like the $n = 6$ prism, with an extra 2-coordinated water molecule inserted into one of the 3-membered rings. RCs of the lowest MKW minimum are given in Table 3. (A different 3D structure was suggested as the lowest minimum in Hartree−Fock calculations of ref 49. Conclusive identification of the heptamer ground state would require, most probably, an extensive search for minimum structures, in conjunction with comparison to experiment.)

## 4. Concluding Remarks

On the basis of a large body of computational studies, including this one, we ask finally a general question: How well can we interpret $H_2O$ properties in terms of molecular interactions? A closely related question is the following: To what extent can we *reproduce* $H_2O$ properties in simulations? A sound zero-order picture of $H_2O$ seems to be available, and one can reproduce quite well gross $H_2O$ features that depend on approximately tetrahedral but flexible hydrogen-bonding (i.e., perfect tetrahedral symmetry of bonding can be distorted at a relatively small energy cost). Examples of such features are reasonable minimum energy structures for different crystalline ice forms and for water cluster isomers, and a sensible liquid structure. However, numerous striking water properties depend on fine details of the PES, which are far from being well understood. Two examples, the ordering ice transition to a ferroelectric structure, and relative energies of cluster isomers, were discussed above; another example, the density maximum of water, is considered in refs 4f and 24a.

There are some obvious ways, in which the presently available PES can be improved. Most of the PES are rigid body; and for some obscure reason, the commonly employed $H_2O$ geometry is the gas phase minimum. Even for the gas phase, vibrationally averaged geometry[41] would make better sense. For condensed phases, elongated OH bonds characteristic of liquid/ice should be used.[32]

A truly realistic treatment should employ flexible monomers. A good flexible water PES is not yet available, although efforts have been made.[4b,5h,25] A common approach is to add to one of the intermolecular PES intramolecular potential terms adopted from $H_2O(g)$. This approach was shown[4b] to reproduce a dramatic decrease in the OH stretch frequency upon formation of hydrogen bonds. (H-bonding stretches OH to a new equilibrium length, which, because of anharmonicity, corresponds to a lower frequency.) However this trick does not work with every PES; furthermore, it is insufficient to reproduce line shapes of the extensively studied and very interesting OH stretch spectra of the different water phases (see, e.g., refs 1, 10, 13, and 25). This is since the force constants and the dipole derivatives depend dramatically on H-bonding in a way which is not yet well understood (e.g., the intramolecular OH···OH coupling, which affects the symmetric−antisymmetric stretch splitting, changes sign upon transition from gas to ice, and the bond dipole derivative increases by 2 orders of magnitude[25]). The recent availability of OH stretch spectra for size selected water clusters[8−10] up to $n = 10$ will certainly boost the efforts to calibrate good flexible PES. Our efforts in this direction[10] are based on the idea of correlating OH bond frequencies with the electric field on H-atoms, following ab initio studies,[46] see end of section 3.2.1.

Improvements in the PES should proceed hand in hand with advances in simulation methodologies, especially, toward a quantum mechanical (QM) treatment. The most common method to simulate water is by classical molecular dynamics or Monte Carlo. However issues such as OH spectra clearly require a QM treatment, since $\hbar\omega \gg k_B T$. The recently measured intermolecular vibrational spectra and tunneling splittings of $H_2O$ clusters are also intrinsically quantum mechanical.[7] But even classical simulations of water at room temperature, or of ice near 273 K, are suspect, since the intermolecular spectrum[1] extends well beyond $k_B T/\hbar$. Under such conditions, dynamics of a QM system can be quite different from that of a classical one. On one hand, the amplitude is enhanced significantly by the zero-point motion; on the other hand, QM energy transfer is restricted by the fact that only discrete quanta are transferred, and zero-point motion is not transferred at all. QM thermodynamics of water has been pursued using PIMC.[24] Calculations of QM dynamics[50] and energy levels[51] in highly anharmonic many body systems such as $H_2O$ and $H_2O$ clusters is currently a very "hot" topic, pursued by a number of groups.

One may note finally a somewhat surprising fact, despite obvious importance of $H_2O$ and a large body of past research, molecular level understanding of $H_2O$ properties is still very incomplete. For example, transport properties of ice are governed by defects.[1,13] While the existence of defects is well established, their molecular structure is poorly known. Transport properties are still interpreted with the help of old venerable models of molecular defect structures, which are certainly oversimplified, and which may well be wrong.[1,52] Another

example is ice surface structure. Icy surfaces play a crucial role in phenomena ranging from ice skating to ozone hole formation. Despite that, molecular surface structure obtained under different physical conditions remains an open subject, which has been currently pursued with renewed interest.[19,53] Vibrational spectra of $H_2O$ ice, liquid, and solid interfaces continue to puzzle researchers;[13,19b,25,54,55] there is much debate on the assignment of the different spectral features. References 13, 19, and 52−55 are but a few examples of recent efforts in the above directions; extensive research continues to be done on molecular properties of $H_2O$. Computer simulations are likely to be instrumental for advancing the understanding of these and other $H_2O$ related phenomena; and such simulations will require ever more refined water PES. Conversely, new things will be revealed on water interactions during the efforts to reproduce observables.

There is still much work to be done for aficionados of this exciting substance.

**Acknowledgment.** V.B. thanks J. P. Devlin for numerous inspiring discussions, and for sharing his deep understanding of ice. R. Whitworth, V. Nield, C. Line, and S. Jackson are gratefully acknowledged for information and discussions on ice order−disorder transition. We thank A. K. Soper for help with neutron diffraction data for the liquid, R. Elber for the configuration overlap routine, and U. Buck for insightful discussions on clusters. This research was funded by a BSF Grant 95-00130, ISF Grant 659/97 (V.B.), and KBN Grant 3 T09A 056 14 (J.S.).

**Supporting Information Available:** Appendices I−IV and a table of energy minima for 16 ordered hexagonal ice structures (8 pages). Ordering information is given on any current masthead page.

## References and Notes

(1) (a) Eisenberg, D.; Kauzmann, W. *The Structure and Properties of Water*; Oxford University Press: New York, 1969. (b) Hobbs, P. V. *Ice Physics*; Clarendon: Oxford, 1974. (c) Stillinger, F. H. *Science* 1980, *209*, 451.

(2) Kawada, S. *J. Phys. Soc. Jpn.* 1972, *32*, 1442. Tajima, Y.; Matsuo, T.; Suga, H. *Nature* 1982, *299*, 810.

(3) (a) Jackson, S. M.; Nield, V. M.; Whitworth, R. W.; Oguro, M.; Wilson, C. C. *J. Phys. Chem. B* 1997, *101*, 6142. (b) Line, C. M. B.; Whitworth, R. W. *J. Chem. Phys.* 1996, *104*, 10008. (c) Jackson, S.; Whitworth, R. W. *J. Phys. Chem. B* 1997, *101*, 6177.

(4) (a) Stillinger, F. H.; Rahman, A. *J. Chem. Phys.* 1978, *68*, 666. (b) Reimers, J. R.; Watts, R. O.; Klein, M. L. *Chem. Phys.* 1982, *64*, 95. Coker, D. F.; Miller, R. E.; Watts, R. O. *J. Chem. Phys.* 1985, *82*, 3554. (c) Jorgensen, W. L.; Chandrasekhar, J.; Madura, J. D.; Impey, R. W.; Klein, M. L. *J. Chem. Phys.* 1983, *79*, 926. (d) Berendsen, H. J. C.; Postma, J. P. M.; van Gunsteren, W. F. *Intermolecular Forces*; Pullman, B. Ed.; Reidel: Dordrecht, 1981; pp 331−342. (e) Berendsen, H. J. C.; Grigera, J. R.; Straatsma, T. P. *J. Chem. Phys*. 1987, *91*, 6269. (f) Cho, C. H.; Singh, S.; Robinson, G. W. *J. Chem. Phys*. 1997, *107*, 7979.

(5) (a) Sprik, M.; Klein, M. L. *J. Chem. Phys.* 1988, *89*, 7556. (b) Ahlstrom, P.; Wallquist, A.; Engstrom, S.; Jonsson, B. *Mol. Phys.* 1989, *68*, 563. (c) Wallquist, A.; Ahlstrom, P.; Karlstrom, G. *J. Phys. Chem.* 1990, *94*, 1649. (d) Zhu, S. B.; Singh, S.; Robinson, G. W. *J. Chem. Phys.* 1991, *95*, 2791. (e) Cieplak, P.; Kollman, P.; Lybrand, T. *J. Chem. Phys*. 1992, *92*, 6755. (f) Kuwajima, S.; Warshel, A. *J. Phys. Chem.* 1990, *94*, 460. (g) Millot, C.; Stone, A. J. *Mol. Phys*. 1992, *77*, 439. (h) Corongiu, G.; Clementi, E. *J. Chem. Phys*. 1992, *97*, 2030. (i) Sciortino, F.; Corongiu, G. *J. Chem. Phys*. 1993, *98*, 5694. (j) Halley, J. W.; Rustad, J. R.; Rahman, A. *J. Chem. Phys*. 1993, *98*, 4110. (k) Rick, S. W.; Stuart, S. J.; Berne, B. J. *J. Chem. Phys.* 1994, *101*, 6141. (l) Bernardo, D. N.; Ding, Y.; Krogh-Jespersen, K.; Levy, R. M. *J. Phys. Chem*. 1994, *98*, 4180. (m) Brodholt, J.; Sampoli, M.; Vallauri, R. *Mol. Phys.* 1995, *85*, 81. (n) Wheatley, R. J. *Mol. Phys*. 1996, *87*, 1083. (o) Dang, L. X.; Chang, T. *J. Chem. Phys.* 1997, *106*, 8149.

(6) Odutola, J. A.; Dyke, T. R. *J. Chem. Phys*. 1980, *72*, 5062.

(7) (a) Liu, K.; Loeser, J. G.; Elrod, M. J.; Host, B. C.; Rzepiela, J. A.; Pugliano, N.; Saykally, R. J. *J. Am. Chem. Soc*. 1994, *116*, 3507. (b) Cruzan, J. D.; Braly, L. B.; Liu, K.; Brown, M. G.; Loeser, J. G.; Saykally, R. J. *Science* 1996, *271*, 59. (c) Liu, K.; Brown, M. G.; Cruzan, J. D.; Saykally, R. J. *Science* 1996, *271*, 62. (d) Liu, K.; Brown, M. G.; Carter, C.; Saykally, R. J.; Gregory, J. K.; Clary, D. C. *Nature* 1996, *381*, 501. (e) Liu, K.; Cruzan, J. D.; Saykally, R. J. *Science* 1996, *271*, 929 and references therein.

(8) Huisken, F.; Kaloudis, M.; Kulcke, *J. Chem. Phys*. 1996, *104*, 17.

(9) (a) Pribble, R. N.; Zwier, T. S. *Science* 1994, *265*, 75. (b) Gruenloh, C. J.; Carney, J. R.; Arrington, C. A.; Zwier, T. S.; Fredericks, S. Y.; Jordan, K. D. *Science* 1997, *276*, 1678.

(10) Buck, U.; Ettischer, I.; Melzer, M.; Buch, V.; Sadlej, J. *Phys. Rev. Lett.* **1998**, *80*, 2578.

(11) Morse, M. D.; Rice, S. A. *J. Chem. Phys*. 1982, *76*, 650.

(12) Pauling, L. *J. Am. Chem. Soc*. 1935, *57*, 2680. For an improvement of the accuracy of the entropy calculation, see: Nagle, J. F. *J. Math. Phys*. 1966, *7*, 1484.

(13) Devlin, J. P. *Int. Rev. Phys. Chem.* 1990, *9*, 29.

(14) (a) Onsager, L. *J. Phys. Chem.* 1939, *43*, 189. (b) Davidson, E. R.; Morokuma, K. *J. Chem. Phys.* 1984, *81*, 3741.

(15) Barkema, G. T.; de Boer, J. *J. Chem. Phys*. 1993, *99*, 2059.

(16) Bjerrum, N. *Science* 1952, *115*, 386.

(17) Sprik, M.; Hutter, J.; Parrinello, M. *J. Chem. Phys.* 1996, *105*, 1142 and references therein.

(18) Tuckerman, M.; Laasonen, K.; Sprik, M.; Parrinello, M. *J. Chem. Phys.* 1995, *103*, 150.

(19) (a) Buch, V.; Delzeit, L.; Blackledge, C.; Devlin, J. P. *J. Phys. Chem*. 1996, *100*, 3732. (b) Rowland, B.; Kadagathur, S.; Devlin, J. P.; Buch, V.; Feldmann, T.; Wojcik, M. *J. Chem. Phys.* 1995, *102*, 8328.

(20) Gregory, J. K.; Clary, D. C. *J. Phys. Chem*. 1996, *100*, 18014.

(21) Sremniak, L. S.; Perera, L.; Berkowitz, M. L. *J. Chem. Phys*. 1996, *105*, 3715.

(22) Smith, P. E.; van Gunstern, W. F. *J. Chem. Phys.* 1994, *100*, 3169 and references therein.

(23) (a) Warshel, A. *Computer Modeling of Chemical Reactions in Enzymes and Solutions*; Wiley: New York, 1991. (b) McCammon, J. A.; Harvey, S. C. *Dynamics of Proteins and Nucleic Acids*; Cambridge University Press: Cambridge, 1987.

(24) (a) Billeter, S. R.; King, P. M.; van Gunstern, W. F. *J. Chem. Phys*. 1994, *100*, 6692. (b) Kuharski, R. A.; Rossky, P. J. *J. Chem. Phys.* 1985, *82*, 5164. (c) Wallqvist, A.; Berne, B. J. *Chem. Phys. Lett.* 1985, *117*, 214.

(25) Whalley, E. *Can. J. Chem*. 1977, *55*, 3429. Rice, S. A.; Bergen, M. S.; Belch, A. C.; Nielsen, G. *J. Phys. Chem.* 1983, *87*, 4295. Wojcik, M.; Buch, V.; Devlin, J. P. *J. Chem. Phys*. 1993, *99*, 2332.

(26) (a) Howe, R. *J. Phys.* 1987, *C1*, 599. (b) Hayward, J. A.; Reimers, J. R. *J. Chem. Phys.* 1997, *106*, 1518. (c) Cota, E.; Hoover, W. G. *J. Chem. Phys*. 1977, *67*, 3839.

(27) It should be noted that our Monte Carlo procedure is not guaranteed to produce all possible structures for a given unit cell. One can compare our results to ref 26a, in which 17 ice structures with eight molecules per unit cell were constructed "manually". We found three structures with $M_{0xy} = 0$, $M_{0z} \neq 0$, 6 with $M_{0xy} \neq 0$, $M_{0z} = 0$, 4 with $M_{0xy} = 0$, $M_{0z} = 0$, and 3 with $M_{0xy} \neq 0$, $M_{0z} \neq 0$, while the corresponding numbers reported in ref 26a are 2/6/4/5, respectively. ($M_{0z}$, $M_{0xy}$ denote dipole components parallel and perpendicular to the interlayer *c*-axis).

(28) Whalley, E. *J. Glaciol*. 1978, *21*, 13.

(29) Kittel, C. *Introduction to Solid State Physics*; Wiley: New York, 1971; Chapters 13, 14.

(30) Becker, R. *Electromagnetic Fields and Interactions*; Blaisdell: New York, 1964. The integral formulas for $N_i$ are given in p 103. $N_i$ can be written as a function of two variables $v_j = F_j/F_i$, $j \neq i$ (e.g., $N_x$ depends on $v_y = F_y/F_x$ and $v_z = F_z/F_x$). Since $v_j$ are close to 1, we used analytical Taylor expansion of $N_i$, up to a third order, in $\delta v_j = v_j - 1$.

(31) Press, W. H.; Flannery, B. P.; Teukolsky, S. A.; Vetterling, W. T. *Numerical Recipes*; Cambridge University Press: Cambridge, 1987; Chapter 10.6.

(32) Kuhs, W. F.; Lehmann, M. S. *Water Sci. Rev*. 1986, *2*, 1.

(33) (a) Anderson, J. B. *J. Chem. Phys.* 1975, *63*, 1499. (b) Anderson, J. B. *J. Chem. Phys.* 1976, *65*, 4121. (c) Suhm, M. A.; Watts, R. O. *Phys. Rep.* 1991, *204*, 293.

(34) (a) Buch, V. *J. Chem. Phys.* 1992, *97*, 726. (b) Sandler, P.; Jung, J.; Szczesniak, M. M.; Buch, V. *J. Chem. Phys.* 1994, *101*, 1378. (c) Sandler, P.; Buch, V.; Sadlej, J. *J. Chem. Phys.* 1996, *105*, 10387.

(35) The water density in the simulation box is 0.97 g/cm$^3$; the reduction with respect to the experimental value 1.00 g/cm$^3$ reflects the reduction of the density of MKW ice minimum with respect to estimated "true" minimum ice density.

(36) (a) Allen, M. P.; Tildesley, D. J. *Computer Simulations of Liquids*; Clarendon Press: Oxford, 1987; Chapter 5. (b) Valleau, J. P.; Whittington, S. G. In *Statistical Mechanics A. Modern Theoretical Chemistry*; Berne, B. J., Ed.; Plenum Press: New York, 1977; Vol. 5, pp 137−168.

(37) (a) Ruocco, G.; Sampoli, M. *Mol. Phys.* 1994, *82*, 875. (b) Neumann, M. *Mol. Phys.* 1983, *50*, 841.

(38) Krynicki, K.; Green, C. D.; Sawyer, D. W. *Faraday Discuss. Chem. Soc*. 1987, *66*, 199.

(39) West, R. C., Ed. *CRC Handbook of Chemistry and Physics*; CRC Press: Boca Raton, 1984; p E-56.

(40) Owicki, J. C.; Scheraga, H. A. *J. Am. Chem. Soc*. 1977, *99*, 7403.

(41) Powles, J. G. *Mol. Phys.* 1981, *42*, 757.

(42) (a) Soper, A. K.; Phillips, M. G. *Chem. Phys.* 1986, *107*, 47. (b) Soper, A. K.; Bruni, F.; Ricci, M. A. *J. Chem. Phys*. 1997, *106*, 247. (c) Narten, F. H.; Levy, H. A. *J. Chem. Phys*. 1971, *55*, 2263.

(43) Sandler, P. General purpose QCLUSTER program for RBDMC simulation of an arbitrary molecular cluster, available via anonymous ftp on cold.fh.huji.ac.il.

(44) (a) Watson, J. K. G. *Mol. Phys*. 1968, *15*, 479. (b) Ernesti, A.; Hutson, J. M. *Chem. Phys. Lett*. 1994, *222*, 257. (c) Eckart, C. *Phys. Rev*. 1935, *47*, 552.

(45) Kabsch, A. *Acta Crystallogr. A* 1976, *32*, 922.

(46) Hermansson, K.; Lingren, J.; Probst, M. M. *Chem. Phys. Lett.* 1995, *233*, 371.

(47) Mas, E. M.; Szalewicz, K. *J. Chem. Phys.* 1996, *104*, 1996.

(48) For example, see: Kim, K.; Jordan, K. D.; Zwier, T. S. *J. Am. Chem. Soc*. 1994, *116*, 11568 and references therein.

(49) Jensen, J. O.; Krishnan, P. N.; Burke, L. A. *Chem. Phys. Lett.* 1995, *241*, 253.

(50) Lobaugh, J.; Voth, A. *J. Chem. Phys.* 1997, *106*, 2400 and references therein.

(51) For example, see: Gregory, J. K.; Clary, D. C. *J. Chem. Phys.* 1996, *105*, 6626. Jung, J. O.; Gerber, R. B. *J. Chem. Phys*. 1996, *105*, 10332. van der Avoird, A.; Olthof, E. H. T.; Wormer, P. E. S. *J. Chem. Phys.* 1996, *105*, 8034. Szabo, D.; Bacic, Z.; Burgi, T.; Leutwyler, S. *Chem. Phys. Lett*. 1995, *244*, 283.

(52) Jonsson, H. *ACS Abstract*; San Francisco, 1997.

(53) Materer, N.; Starke, U.; Barbieri, A.; van Hove, M. A.; Somorjay, G. A.; Kroes, G. J.; Minot, C. *J. Phys. Chem*. 1995, *99*, 6267.

(54) Du, Q.; Superfine, R.; Freysz, E.; Shen, Y. R. *Phys. Rev. Lett.* 1993, *70*, 2313.

(55) Li, J. C.; Leslie, M. *J. Phys. Chem*. 1997, *101*, 6304. Klug, D. D.; Tse, J. S.; Whalley, E. *J. Chem. Phys*. 1991, *95*, 7011.